Simulation of the Great Bay Estuarine System: Tides with Tidal Flats Wetting and Drying

Ş.N. Ertürk, **A. Bilgili** , **M.R. Swift**, **W.S. Brown**, **B. Çelikkol**

University of New Hampshire,

Durham, New Hampshire, 03824, U.S.A.

J.T.C. Ip, **D.R. Lynch**

Dartmouth College,

Hanover, New Hampshire, 03755, U.S.A.

March 8, 2001

To be submitted to Journal of Geophysical Research

Abstract

Realistic lunar tides of the Great Bay Estuarine System have been simulated using a fixed-boundary finite-element numerical model as described in Ip *et al.* (1998). It is a two-dimensional, nonlinear, time-stepping model with a ground water component coupled to a kinematic force balance to facilitate the realistic drainage and filling of elements during ebb and flood respectively. The numerical model reproduces the observed M_2 tides as described in Swift and Brown (1983), and it successfully captures qualitatively the correct residual currents and transports, realistic mass-conserving flooding and dewatering of the tidal flats, and the current asymmetry between flood and ebb. The simulation results were sensitive to local bathymetry and the implemented friction law. The accuracy of the model is demonstrated by comparison with the 1975 Great Bay study (Swift and Brown, 1983) in terms of tidal elevations at 14 tidal stations and 4 cross-sectionally averaged current measurements in the estuary. Quantitatively the model results show good agreement with observations, displaying correlation coefficients of ≥ 0.96 in surface elevation, ≥ 0.95 in averaged current, with RMS errors of ≤ 0.20 m and ≤ 0.45 m/sec respectively. In addition, tidal flat hydrodynamics, characteristic distributions of residual current, sediment bedload transport, and the influence of topography on the overall circulation in the region are also discussed.

Keywords: Finite elements, tidal flats wetting and drying, nonlinear kinematic model, sea levels, currents, model comparison with observations, M_2 tide, Great Bay Estuarine System, New Hampshire coast.

1 Introduction

Tidal currents and surface elevation changes dominate the physical oceanographic features of typical shallow embayments. For cases where the tidal range is on the order of the mean depth, the physics are strongly nonlinear, and asymmetry in flood or ebb current strength can cause net transport of sediment, nutrients and pollutants. These conditions can occur in small inlets opening directly to the ocean but more often are found in tidal channels connecting larger bodies of water. In both cases, highly nonlinear tidal flows can fill and empty shallow basins which often have large expanses of tidal flats at low water.

In this paper, we describe the application of a new model to the Great Bay Estuary, New Hampshire (Figure **??**), which is located in the western Gulf of Maine. The typical 2.5 m tidal sea level excursions of the Gulf of Maine cause approximately 40% of the volume of Great Bay to be exchanged each tidal cycle. The Gulf of Maine connects to the inner estuary by way of the Lower Piscataqua River, whose channel depth is typically 15 m with maximum currents that range from 0.5 to 2.0 m/sec. Most of the water on each tidal cycle enters Little Bay, because the Upper Piscataqua River is relatively shallow. The inner estuary consists of Little Bay and Great Bay, with depths in the main channels on the order of 10 m, with maximum currents of approximately 0.5 m/sec. Several rivers empty into Little Bay and Great Bay. Normally the ratio of river discharge to tidal prism is less than 1%. Consequently, tidal currents are much larger than the steady, density-driven circulation and the system is well-mixed.

In the Great Bay Estuary the M_2 constituent is dominant over the two other semi-diurnal constituents N_2 and S_2 by an order of magnitude. Also, the two important diurnal constituents K_1 and O_1 are of lower order. Swift and Brown (1983) suggest that the confluence of Lower Piscataqua, Upper Piscataqua, and Little Bay at Dover Point appears to act like a hydraulic choke which separates the Great Bay Estuary into two dynamic regimes. The tidal flow in the Lower Piscataqua regime is relatively more dissipative with decreasing amplitude and increasing phase landward – a progressive wave characteristic. The flow in the Little Bay/Great Bay regime is less dissipative and has an increasing amplitude and little phase change – a standing wave characteristic.

The inner estuary, particularly Great Bay, has extensive tidal flats. The flooding and drying of such tidal flats pose significant modeling problems. A common numerical modeling approach is

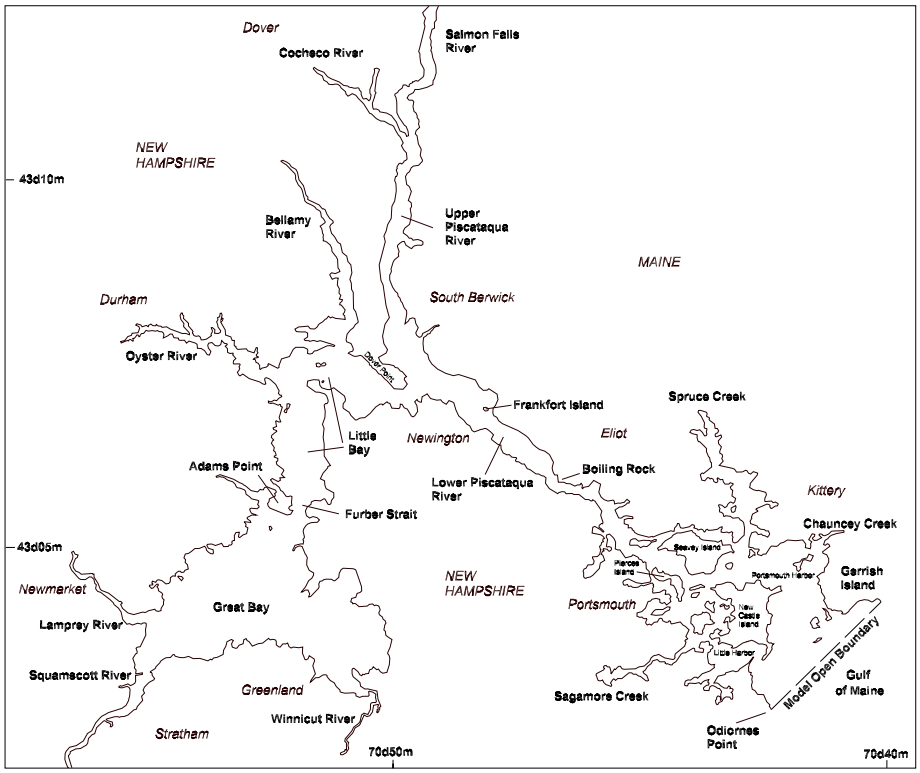

Figure 1: A location map of the Great Bay Estuarine System. (– – – – –) denotes model open boundary.

to "turn off" model grid elements, when the model surface elevation drops below a prescribed threshold (see Lin and Falconer, 1997). An alternate method employed by Ip *et al.* (1998) for a drying tidal flat on a horizontally two-dimensional finite element grid, has the water surface recess into a sediment layer characterized by Darcian flow. Thus the ground water dynamics, governed by a simple diffusion process, even when the overlaying water has receded. In this approach, the In this approach, the finite element grid does not change shape and retains all the computational advantages of a fixed grid. call ADAM, was implemented by Ip *et al.* (1998) for a series for a series of geometrically prescribed, generic channel/flat cross-sections and for a portion of Great Bay. The Ip *et al.* (1998) The Ip *et al.* (1998) application of the ADAM algorithm demonstrated numerical robustness and gave qualitatively correct simulations of the semi-diurnal tidal response. Herein we apply ADAM to the entire Great Bay Estuary, adding detailed bathymetry of the whole system, and a depth-dependent bottom friction coefficient. We took great care at this stage because preliminary experiments showed that model simulation

results were very sensitive to these issues. We focus on M_2 sea level forcing at the Gulf of Maine open ocean boundary. Model performance has been evaluated through comparison with tidal predictions based on a suite of current and surface elevation observations from the 1975 Great Bay study described by Swift and Brown (1983). A summary of those observations is presented next.

2 Description of Observations

During the summer of 1975 a comprehensive field program to measure the tidal elevations and currents within the Great Bay Estuarine System was conducted by the University of New Hampshire (UNH) in cooperation with the National Ocean Survey (NOS). UNH investigated the vertical and horizontal variability of estuarine currents and water properties at a selected set of strategic locations in the estuary. NOS deployed an array of sea level and current measurement stations covering the estuary. Swift and Brown (1983) used current observations and transports estimated from sea level observations to produce estimated cross-section averaged transports at four locations in the estuary (Figure **??**). Those observations are briefly discussed here.

2.1 Current Observations

The NOS current time series were measured at locations shown in Figure **??**. A typical mooring consisted of an anchored surface flotation unit, from which were suspended a string of Savonius rotor current meters and a heavy weight to minimize the current-induced tilt of the array. The nominal depths of the current measurements used were 4.6 m and 9.2 m. Every l2 minutes, five current speeds and five current directions were sampled at 1-second intervals, telemetered to the NOAA (National Oceanic and Atmospheric Administration) ship FERREL, and then recorded on magnetic tape aboard the surface flotation unit. Any data pair whose direction fell outside $\pm 15^\circ$ of the mean direction were discarded. The remaining speeds and directions were averaged to form the vector assigned to that particular 12-minute sample. The estimated precision of the measured current speed and direction are ± 2.6 cm/sec and $\pm 2.5^\circ$ respectively for zero tilt and speeds less than 52 cm/sec. The estimated precision of speeds greater than 52 cm/sec is about ± 5.0 cm/sec.

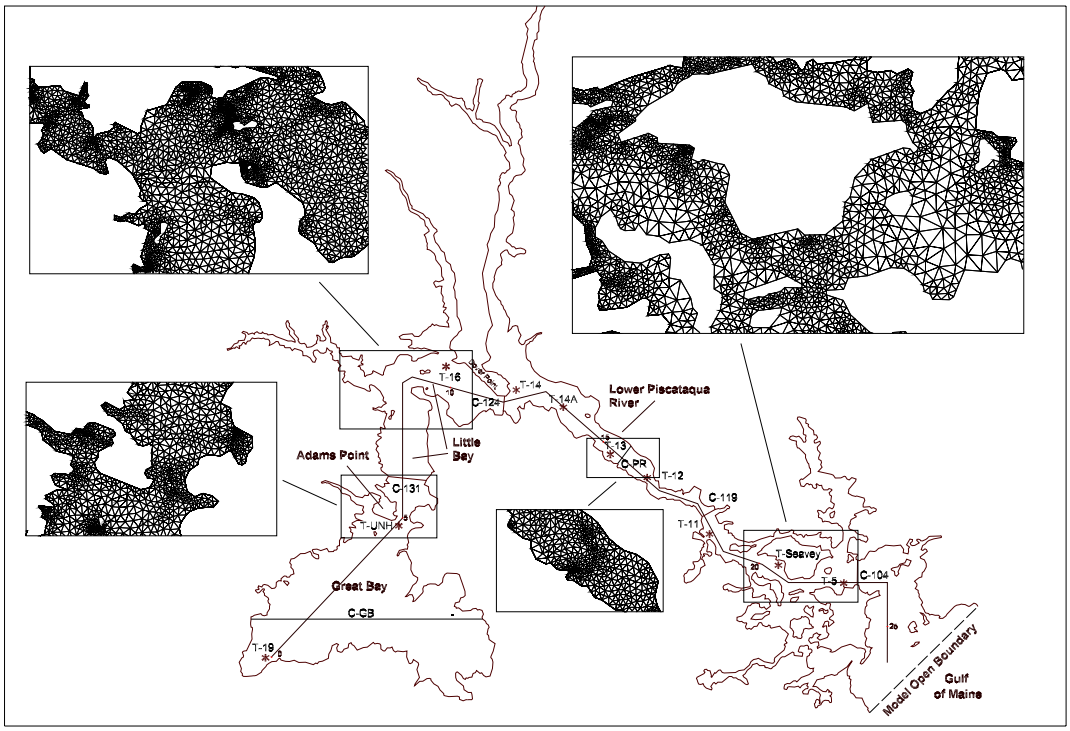

Figure 2: Observation stations along the Great Bay Estuarine System (`gbes10` mesh). The detailed finite element mesh is shown at four selected areas. T indicates a tidal elevation gauge and C indicates a current meter section except C-PR and C-GB, which are example bathymetry sections.

2.2 Sea Level Observations

The NOS deployed an array of automatic digital recording (ADR) tidal gauges at the locations of the sea level stations indicated in Figure **??**. The ADR tidal gauges recorded 6-minute values of the sea level, as measured by a float in the standard NOS tidal well to a resolution of 3 cm. The UNH also measured Adams Point sea level with a Metritape Sea Level Sensor – a hydrostatic pressure-actuated, waterproof precision-wound resistance helix inserted in a tidal well to damp high frequency sea level fluctuations. The output voltage was recorded every half-hour with an estimated short term equivalent sea level precision of ± 0.5 cm and a long term precision of ± 2.0 cm.

A harmonic analysis (Dennis and Long, 1971) of the sea level records showed that the dominant M_2 semi-diurnal constituent amplitude decreases from 1.29 m at the open ocean proxy station T-5 to 0.94 m (T-14) at the Dover Point confluence of the Lower Piscataqua, Upper Piscataqua, and Little Bay and increases throughout Little and Great Bays to the head of the inner estuary at T-19 (Figure **??**). The 76° M_2 phase lag of the T-19 Great Bay sea level relative to the open ocean boundary sea level explains most of the corresponding 2.5 hours time lag of total sea level.

2.3 Cross-Section Averaged Currents

Swift and Brown (1983) describe how currents and sea levels were aggregated to form estuarine cross-section averaged longitudinal current time series at the sites shown in Figure **??**. Observed cross-section averaged current is based on vertically averaged current measurements made at a single mooring at each cross-section. Two multipliers were applied to the axial component of the vertically averaged, station time series – one for the flood and one for the ebb. The multipliers were determined such that the net transport over the particular phase (flood or ebb) agreed with the cumulative tidal prism inland of the cross-section. Prism was estimated using nautical charts and average tidal ranges. The harmonic constants for the astronomical M_2, S_2, N_2, K_1, and O_1 tidal constituents, as well as the nonlinear shallow water constituents of M_4 and M_6 were determined by a harmonic analysis of these cross-section averaged current time series. The estimated uncertainty of the cross-section averaged currents is $\pm 10\%$.

3 Numerical Model Description

We adopted the fixed-domain finite-element kinematic (that is, without local and advective accelerations) model ADAM developed by Ip *et al.* (1998) to simulate the M_2, M_4, and M_6 tides in the Great Bay Estuary. This kinematic numerical model offers efficient and high resolution numerics for simulating physically realistic flooding and dewatering of tidal flats in shallow embayments. In this approach the water column is being modeled as a composite system of open channel with a porous medium sublayer beneath it and above the bedrock, as shown in Figure **??**. The force balance in shallow narrow tidal embayments can be dominated by bottom friction and pressure gradient (Friedrichs *et al.*, 1992). This balance has been verified observationally throughout much of the Great Bay system by Swift and Brown (1983). In particular, acceleration term magnitudes were approximately 12% that of either the pressure gradient or stress terms for deep water channel segments. Since much of the remaining estuary is shallow, better agreement throughout the whole system was anticipated. Additionally, we neglect Coriolis accelerations because of the relatively small length scale of our Estuarine System. Since observations show the estuary to be vertically-mixed, we are justified in using a simplified 2-d depth-averaged assumption. Thus the depth-averaged kinematic equations are employed to model the flow in the open channel. Flow in the sub bottom porous medium is described by Darcy's law (Roberson *et al.*, 1988).

With the forementioned assumptions, the governing equations are

Continuity:

$$\frac{\partial H}{\partial t} + \nabla \cdot H\mathbf{v} = 0 \tag{1}$$

Horizontal momentum:

$$gH\nabla\zeta + c_d|\mathbf{v}|\mathbf{v} = \mathbf{0} \tag{2}$$

where H is the total depth of the water column, $\mathbf{v}$ is the depth-averaged velocity, t is time, ∇ is the horizontal gradient differential operator, ζ is the surface elevation relative to a horizontal datum, g is the acceleration of gravity, c_d is the bottom drag coefficient. To better approximate a realistic estuarine bottom, we adopted the Manning formula of parameterizing a depth dependent bottom friction coefficient in the form:

$$c_d = \frac{gn^2}{H^{1/3}} \tag{3}$$

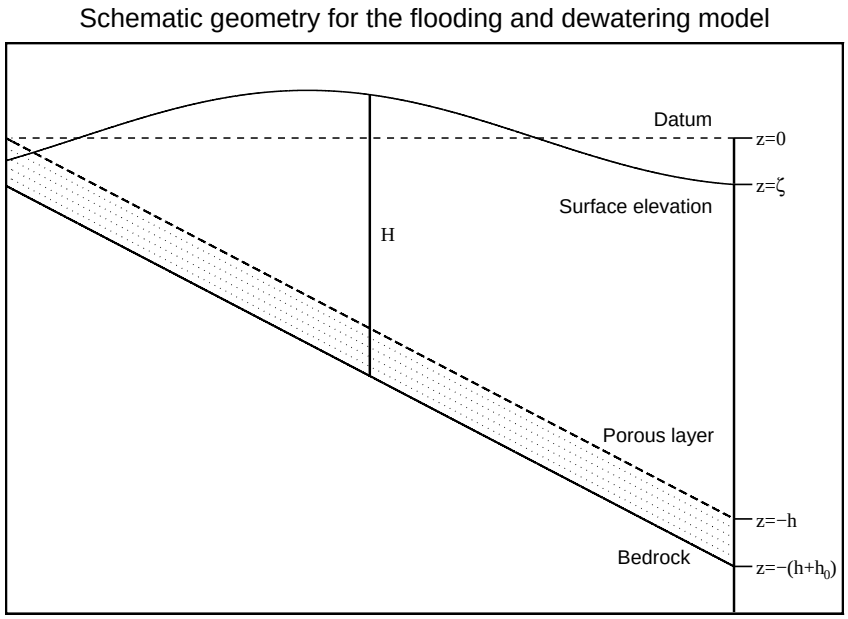

Figure 3: Schematic geometry for the flooding and dewatering model (Ip *et al.*, 1998).

where n is the Manning bottom roughness coefficient.

Substituting the kinematic momentum balance into continuity and incorporating the Darcian description for the porous medium sublayer, the governing equations for the composite system are reduced to a scalar nonlinear diffusion equation of the form:

$$S\frac{\partial \zeta}{\partial t} - \nabla \cdot \mathcal{D}\nabla\zeta = 0 \tag{4}$$

in which the storage coefficient S and the nonlinear diffusion coefficient $\mathcal{D}$ are specified as functions of H. For our system,

$$S = \begin{cases} 1 & \text{if } H > h_0 \\ \varepsilon & \text{if } H \leq h_0 \end{cases} \tag{5}$$

$$\mathcal{D} = \begin{cases} \kappa h_0 + (H - h_0)^{3/2}\sqrt{\frac{g}{c_d|\nabla\zeta|}} & \text{if } H > h_0 \\ \kappa H & \text{if } H \leq h_0 \end{cases} \tag{6}$$

where the total depth, $H = h + h_0 + \zeta$, h is the bathymetric depth, and h_0 is the thickness of the porous medium with porosity ε and hydraulic conductivity κ.

This nonlinear diffusion equation (**??**) is discretized on linear finite elements using the Galerkin weighted residual method in space. Conventional finite differences are applied for the time

integration:

$$S^{k+\theta}\left[\frac{\zeta^{k+1}-\zeta^{k}}{\Delta t}\right]-\nabla\cdot\mathcal{D}^{k+\theta}\nabla\left[\theta\zeta^{k+1}+(1-\theta)\zeta^{k}\right]=0 \tag{7}$$

with time level k and time weighting factor theta in the range $0 \leq \theta \leq 1$. An implicit solution ($\theta = 1$) is obtained iteratively in each time step, as described in Ip *et al.* (1998).

4 Simulations

4.1 Computational Setup

Figure **??** displays example sections of the computational mesh (named `gbes10`) that we constructed from available bathymetry for the Great Bay Estuarine System. The finite element domain boundary corresponding to the mean water level (datum) was digitized from the USGS (United States Geological Survey) topographic maps and the domain was discretized using linear triangular elements (see Figure **??**). The horizontal coordinates of the mesh were converted from latitude-longitude to meters using the New Hampshire State Plane Coordinate System, according to the NAD83 datum. The tributary rivers in Great Bay were not included in the computational grid because of their minimal effect on the overall estuarine circulation. These were edited out at locations where they intersect with Great Bay and treated as shoreline boundaries. The resultant mesh has 22140 nodes and 39617 elements. All elements have areas less than 4500m^2 with inside angles larger than 33 degrees. The grid resolution δ (estimated by $\delta \approx \sqrt{2A_e}$ with element area A_e) is in the range, 4.72 m $\leq \delta \leq$ 204.66 m with an average δ of 47.91 m. A sensitivity study of element size revealed that further refinement of the current elements did not offer a noticeable effect on the present results. The nodal bathymetries were interpolated from a data set digitized from the U.S. NOAA navigational charts, supplemented by UNH measurements in areas where NOAA data were not available. The domain bathymetry consists of a deep center channel, surrounded by tidal flats, running along the estuary from the mouth to the middle section of Great Bay. In Great Bay, this main channel branches into two shallow channels towards the mouths of the Squamscott and Winnicut rivers. Figure **??** shows bathymetric profiles of the Swift and Brown (1983) current cross-sections (C-104, C-119, C-124 and C-131), as well as two additional cross-sections in the Piscataqua River (C-PR) and Great Bay (C-GB). The large percentage of tidal flats in Little Bay (C-131) and Great Bay (C-GB) shows the importance of flooding and dewatering processes in determining the overall estuarine

Constituents	**Amplitudes** (m)	**Phases** ($^\circ G$)
M_2	1.290	102
M_4	0.013	353
M_6	0.005	161

Table 1: The harmonic constants for the M_2-M_4-M_6 forcing constituents across the open ocean boundary.

circulation.

M_2, M_4, and M_6 tidal forcing is specified as a Dirichlet elevation boundary condition across the open ocean boundary extending from Gerrish Island to Odiornes Point (see Figure **??**). The elevation time series used to force the model at the open ocean boundary was predicted using the harmonic constants shown in Table **??**. These are derived from two offshore stations near Boon Island, Maine (43.120° N, 70.410° W) and Hampton, New Hampshire (42.900° N, 70.785° W).

A constant Manning's roughness coefficient, n, of 0.035 was used throughout the estuary. The upper limit for the maximum bottom friction coefficient was fixed at 0.060, restricting the friction coefficient to values not exceeding the empirical maximum friction coefficient reported by Swift and Brown (1983). All the simulation parameters are summarized in Table **??**.

The simulation was started with the fluid at rest at high tide at 00:00:00 28 August 1975. The simulation was terminated after six M_2 cycles – one tidal cycle after dynamical equilibrium had been established. Time series of velocities and surface elevations and the residuals of tidal velocity and a representation for sediment transport were generated and analyzed at the completion of the simulation.

4.2 Model Results:

4.2.1 M_2 Tidal Sea Levels and Currents

As shown in Figure **??**, model M_2 sea level amplitudes decrease moving landward in the Piscataqua River, while amplitudes at locations in Little/Great Bay stay relatively uniform. Figure **??** also shows the simulated M_2 sea level phases, which increase with distance into the estuary.

Description	**Parameters**
x-dimension	360 km $\leq x \leq$ 381 km
y-dimension	60 km $\leq y \leq$ 80 km
Grid resolution	4.72 m $\leq \delta \leq$ 204.66 m
Average grid resolution	δ =47.91 m
Bathymetry range	-1.17 m $\leq h \leq$ 24.69 m
Porous layer thickness	$h_0 = 1.0$ m
Hydraulic conductivity	$\kappa = 3.162 \times 10^{-4}$ m/sec
Minimum porosity	0.35
Manning's roughness coefficient	0.035
Bottom friction coefficient range	$0.004 \leq c_d \leq 0.060$
Time increment	$\Delta t = 111.78$ sec
Time steps per M_2 period	400
Tidal periodicity	$T = 12.42$ hrs
Length of simulation	$0 \leq t \leq 6T$
Numerical implicity	$\theta = 1$
Number of nonlinear iterations	7

Table 2: Simulation parameters for M_2-M_4-M_6 tidal flow simulation on the `gbes10` mesh.

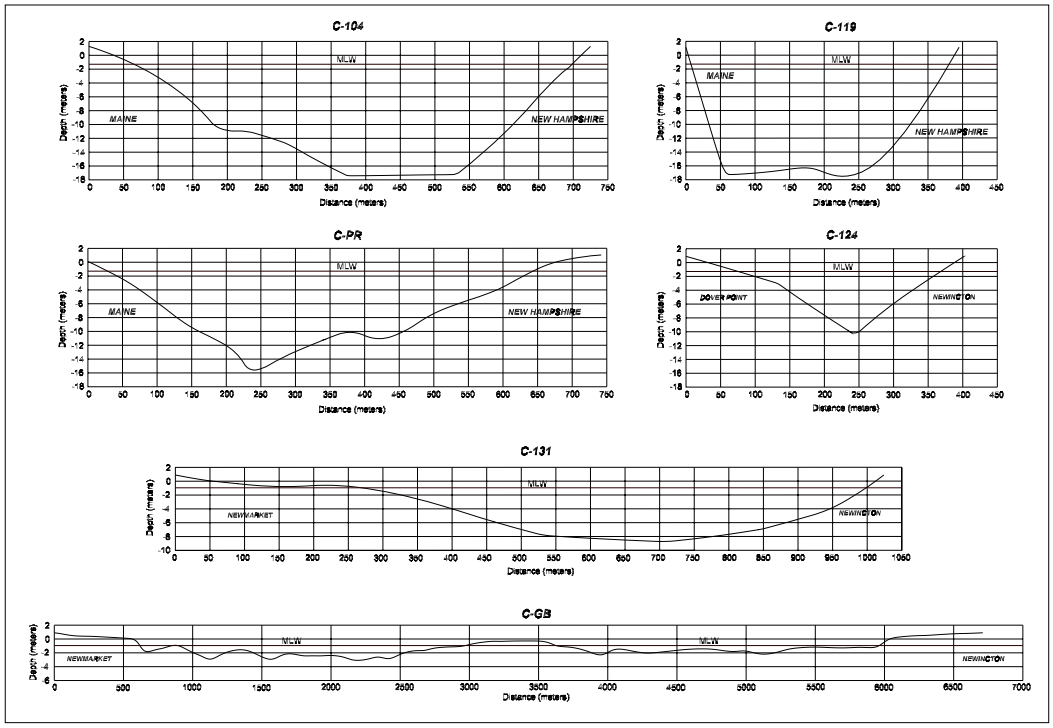

Figure 4: Detailed cross-sections along the Great Bay Estuary (`gbes10`) shown at six selective transects.

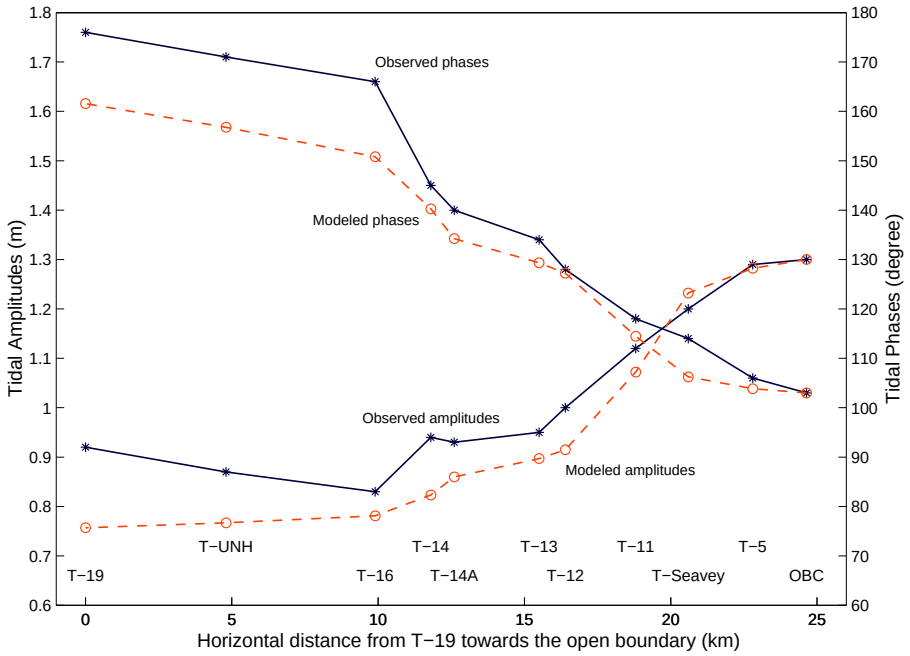

Figure 5: Comparisons of M_2 amplitudes and Greenwich phases of surface elevations at the 10 observation stations.

This increase however, is much larger in the Piscataqua River region than in the Little/Great Bay regions. While both model M_2 amplitude and phase distributions show good agreement with Swift and Brown (1983) results and with the observed character of the tidal wave in the estuary, there are differences. In particular the observed amplitude and phase increase in the Little Bay/Great Bay regime is not modeled correctly. Those differences are highlighted in the following time series intercomparisons.

4.2.2 Comparisons between Model and Observed Time Series

While model forcing at the mouth boundary condition is dominated by the M_2 constituent surface elevation, the model nonlinearities generate higher harmonics in the form of M_4 and M_6 contributions. Thus model sea level and current simulations at the observation sites are compared with hindcast time series based on the M_2, M_4 and M_6 harmonic constants given by Swift and Brown (1983).

The results for surface elevation show excellent agreement at Station T-5 as expected because it is so near the model open boundary. In the Lower Piscataqua regime the model and observed

phases compare well, but the model underpredicts the amplitudes slightly (Figure **??**). In the Little Bay-Great Bay regime the model and observation differences are greater with the model underprediction of amplitude being visually evident. The model amplitude response appears to have too much dissipation, but phase error is small relative to amplitude error. Tidal elevation observations upriver, however, tend to have more extreme peaks and troughs compared to the model predictions. The timing of high water and low water, on the other hand, is comparatively better. These characteristics are reflected in the Table **??** summary of comparison statistics.

Since the seaward end of the system is most influenced by the M_2 constituent and the boundary condition is set to match observed forcing, better surface elevation correspondence near the mouth is expected. Nonlinear effects due to bottom friction and changing geometry are probably greater upriver. The influence of nonlinearities, and the associated production of M_4 and M_6 contributions, in general provide greater potential for discrepancies between theory and observations. The absence of an acceleration term in the ADAM model may also be a factor. Including the S_2 constituent to the boundary forcing was also tried but with no improvement.

The model-simulated cross-section averaged currents (Figure **??**) were calculated by spatially averaging the longitudinal component of current across the channel. Overall, the agreement between predicted and observed currents is good. The plots do not indicate a consistent pattern of discrepancy. Differences could be due to local conditions at the current meter mooring site, errors introduced during field current data processing, as well as the model's ability to resolve flow details. Table **??** summarizes current time series comparison statistics.

4.2.3 Residuals

The real and model estuaries are nonlinear, thus non-tidal "residual" currents are revealed by averaging results over an M_2 tidal cycle. Those results are reviewed in this section.

Residual Velocity

In this study, the residual velocity, $\mathbf{v_r}$, is defined as:

$$\mathbf{v_r} = \frac{1}{T}\int_0^T \mathbf{v}dt \tag{8}$$

where $\mathbf{v}$ is the model tidal velocity and T is the M_2 tidal period (12.42hrs). The magnitudes of the current residual vectors decrease considerably going upriver, probably due to a combination

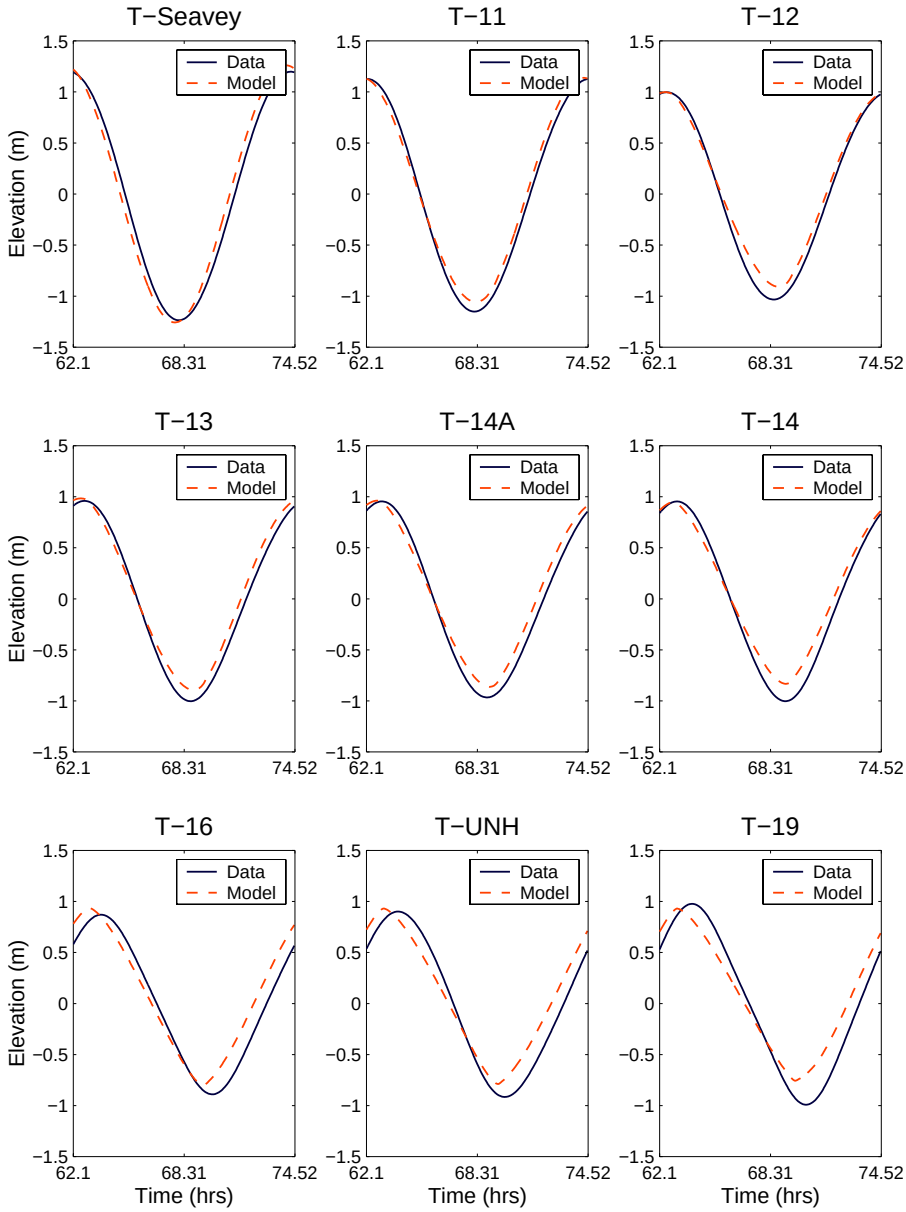

Figure 6: Comparisons of surface elevations at 9 tidal stations.

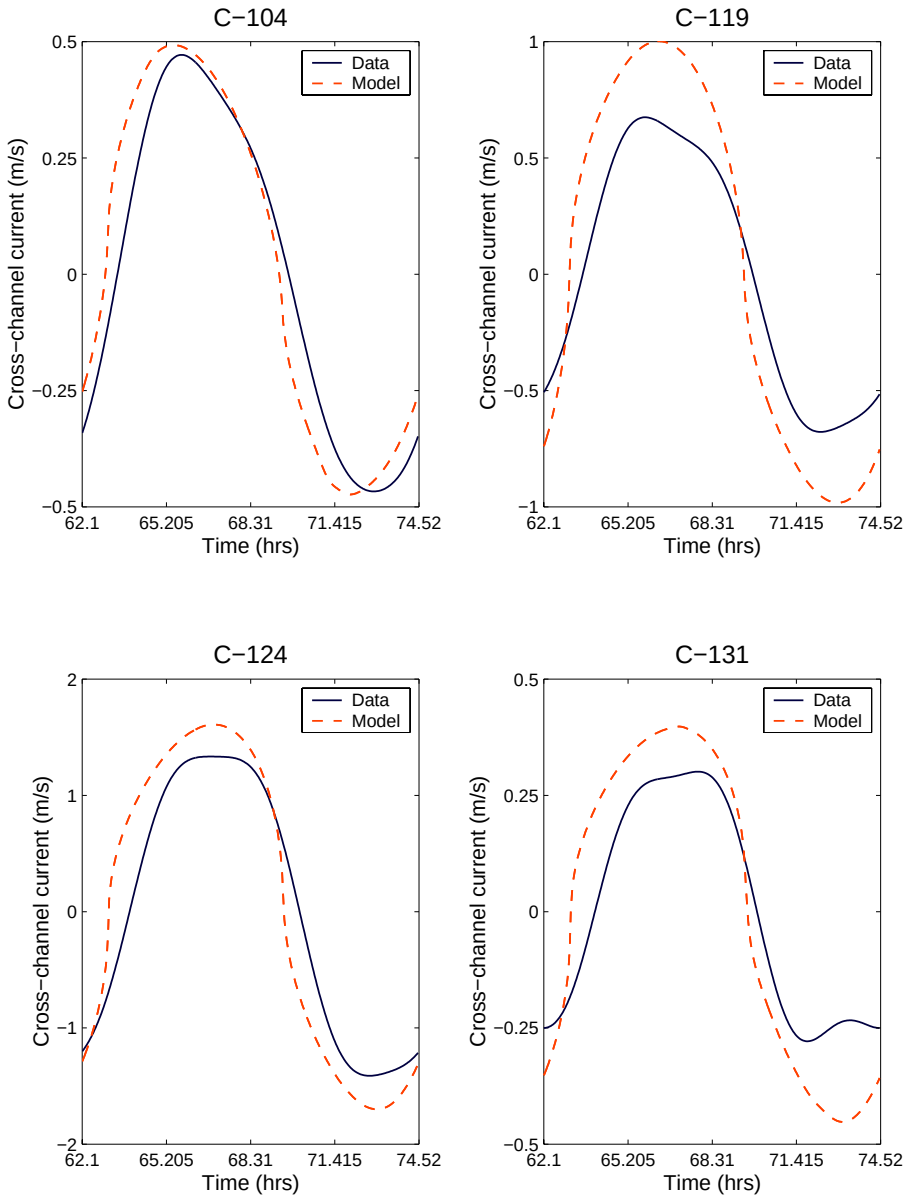

Figure 7: Comparisons of cross sectionally averaged velocities at 4 locations.

Station I.D.	C	E_+	E_-	**RMS**	**nRMS**	S
C-104	0.961	+0.185	−0.258	0.114	0.335	0.889
C-119	0.980	+0.332	−0.460	0.322	0.633	0.600
C-124	0.957	+0.777	−0.942	0.455	0.423	0.821
C-131	0.950	+0.217	−0.254	0.144	0.633	0.600
T-5	0.999	+0.063	−0.057	0.041	0.044	0.998
Seavey	0.990	+0.173	−0.177	0.134	0.154	0.976
T-11	0.997	+0.097	−0.109	0.083	0.103	0.989
T-12	0.998	+0.064	−0.186	0.066	0.091	0.992
T-13	0.995	+0.089	−0.143	0.100	0.142	0.980
T-14A	0.992	+0.118	−0.169	0.111	0.165	0.973
T-14	0.995	+0.114	−0.218	0.109	0.160	0.974
T-16	0.962	+0.148	−0.293	0.182	0.303	0.908
T-UNH	0.966	+0.211	−0.280	0.180	0.287	0.918
T-19	0.965	+0.240	−0.355	0.200	0.301	0.910

Table 3: Summary of comparison statistics. C is the correlation coefficient, E_+ is the maximum positive error, E_- is the maximum negative error, **RMS** is the root mean square error between observation and model results, **nRMS** is the RMS error normalized by the root mean square of the observations, and S is the skill defined by $S = 1 - (nRMS)^2$.

of decreasing progressiveness of the tidal wave and generally lower current velocities. This decrease is especially important around Dover Point (T-14) beyond which the tidal wave starts showing standing wave characteristics (see Figure **??**).

Where intertidal areas can be found adjacent to relatively deep main channels, in Little Bay (Figures **??**), the Piscataqua River and on the north-eastern side of New Castle Island, residual velocity vectors are generally directed in flood direction over the tidal flats and in the ebb direction in the main channels. The flood-oriented residual velocities are much weaker than the ebb oriented ones. Such a residual velocity pattern suggests a flood dominance in the drying areas and an ebb dominance in the main flow channels. The area between the 3m and 7m isobaths appears to be the zone where the transition from the flood- to ebb-dominance occurs. This transitional area is characterized by small scale eddies where exchange between flood dominant and ebb dominant areas takes place.

The landward transition from ebb to flood dominance may be due to the partially progressive nature of the tidal wave, which is characterized by flood currents at the crest (as well as ebb currents at the trough). Over shallow areas, the flooding current at high water dominates since the low water ebb is more restrained by bottom friction or may be missing all together due to drying. The net volume transport into the estuary over the shallow boundary areas must then be balanced by outward residual current in the main channel. Similar situations have also been observed in other estuaries that are shallow with respect to their tidal range (see Friedrichs *et al.*, 1992, Bowers and Al-Barakati, 1997, Li and O'Donnell, 1997). Further evidence that this pattern is a basic feature is provided by the similar results of ADAM applications to a series of geometrically defined test cross-sections described by Ip *et al.* (1998).

Figures **??** shows the residual current pattern in the southwest corner of Great Bay. The model residual current vectors over the extensive Great Bay mudflats are generally directed towards the relatively shallow main channel, which shows ebb-dominance (Figures **??**). This convergence results in several relatively large-scale gyres on the lower portions. On the northern section, where the channel depth is deeper, there is a trend similar to the one explained above for the case of intertidal areas adjacent to deeper channels. An along shore flood dominant residual velocity pattern is also noted in areas close to the shoreline at the lower sections.

In the shallow back channels on the southwestern side of New Castle Island, the velocity residuals are mostly flood oriented, except in Sagamore Creek. These may be functioning as the shallow

flood-dominant tidal flats with respect to the deeper ebb-dominant main channel, although separated by New Castle Island.

Residual Bedload Sediment Transport

Due to strong tidal currents, the bottom sediments of the main channel of the Great Bay Estuarine System consist mainly of coarse sands and gravel (Armstrong *et al.*, 1976). Thus bedload transport is an important mechanism of sediment movement. While there is a wide range of bedload transport models available which take into account grain size, density, bottom shear stress and current speed (see Yalin, 1977, Simons and Senturk, 1977, and Garde and Ranga Raju, 1985), in most of these, bedload flux is taken to be proportional to bottom friction and/or current to some power (see Van de Kreeke and Robaczewska, 1993 and Jago and Mahamod, 1999). In this study, we define a "residual sediment transport vector", $\mathbf{t_r}$, to characterize the hydrodynamic potential of the flow to induce net bedload transport without reference to specific sediments. The vector, $\mathbf{t_r}$, defined by

$$\mathbf{t_r} = \frac{1}{T}\int_0^T |\mathbf{v}|^2 \mathbf{v} dt \tag{9}$$

where $\mathbf{v}$ is the model tidal velocity and T is the tidal period, is proportional to the average power per area exerted by the flow on the bottom. This power is then available to initiate and sustain benthic movement of non-cohesive sediment particles. While not actually equal to sediment-specific bedload flux quantitatively, the residual sediment transport vector will enable us to infer the direction and relative magnitudes of potential transport.

Figures **??**, **??**, **??**, and **??** illustrate the model residual bedload sediment transport pattern at dynamical equilibrium. It is observed that all of the residual sediment transport vectors are oriented towards the inner estuary at upper estuary locations beyond Dover Point, suggesting an upriver transport of coarse sediments (Figures **??** and **??**). The magnitudes are several orders higher in Little Bay than in Great Bay, with strong southward sediment transport occurring in Furber Strait (Figure **??**). This suggests Little Bay as an immediate coarse sediment supply for Great Bay. The magnitudes are also higher in the center channel than on the tidal flats. The transport due to tidal action is almost stagnated on the mudflats of Great Bay, with a very small flood oriented movement towards the land.

Near the Dover Point intersection of Little Bay and the Piscataqua River, there is flood-oriented transport on the flats and ebb-oriented transport in the center channel. Around the southern side

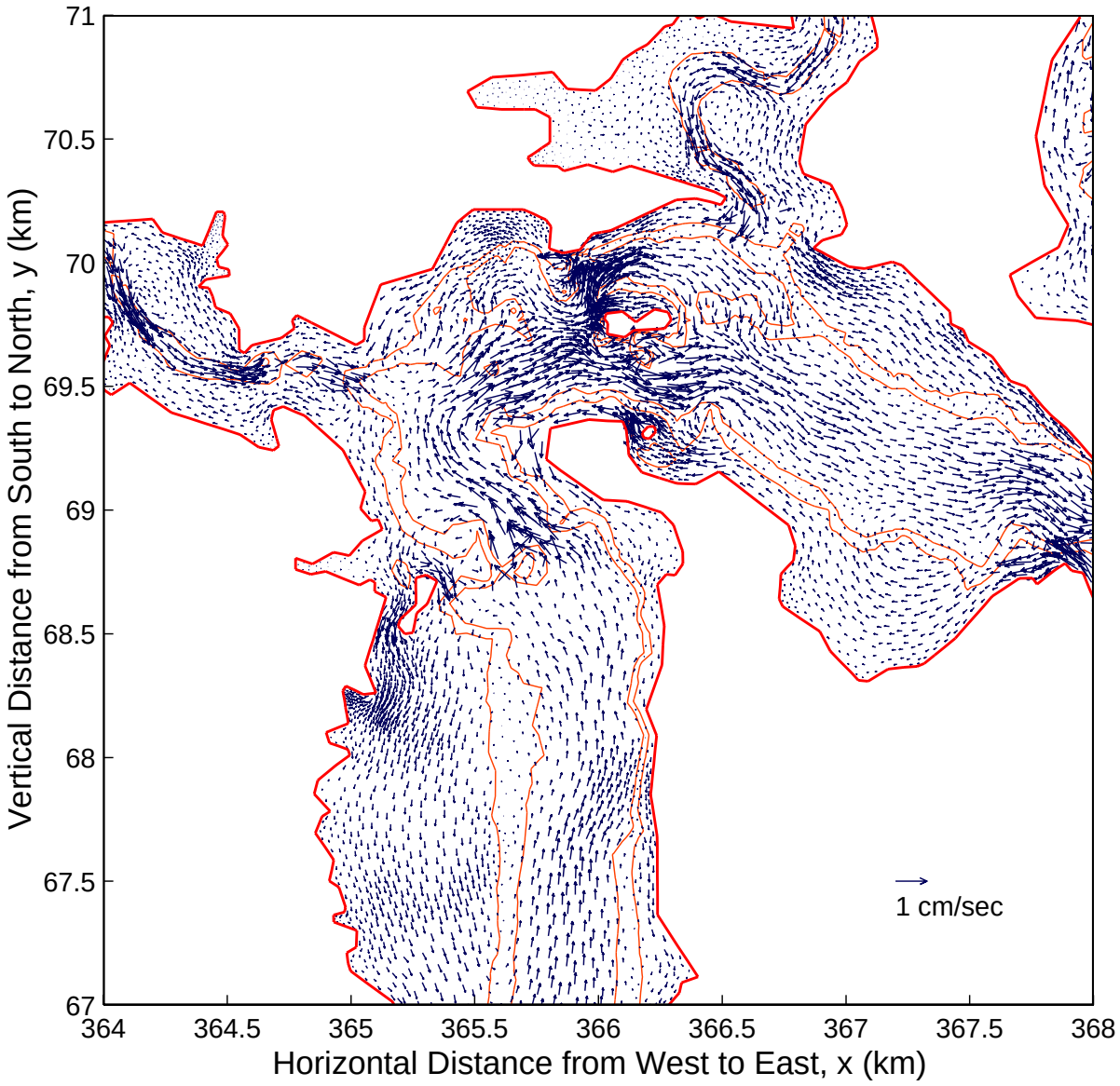

Figure 8: Residual M_2 velocity in Little Bay. The inner isoline is the 7 m isobath and the outer is the 3 m isobath.

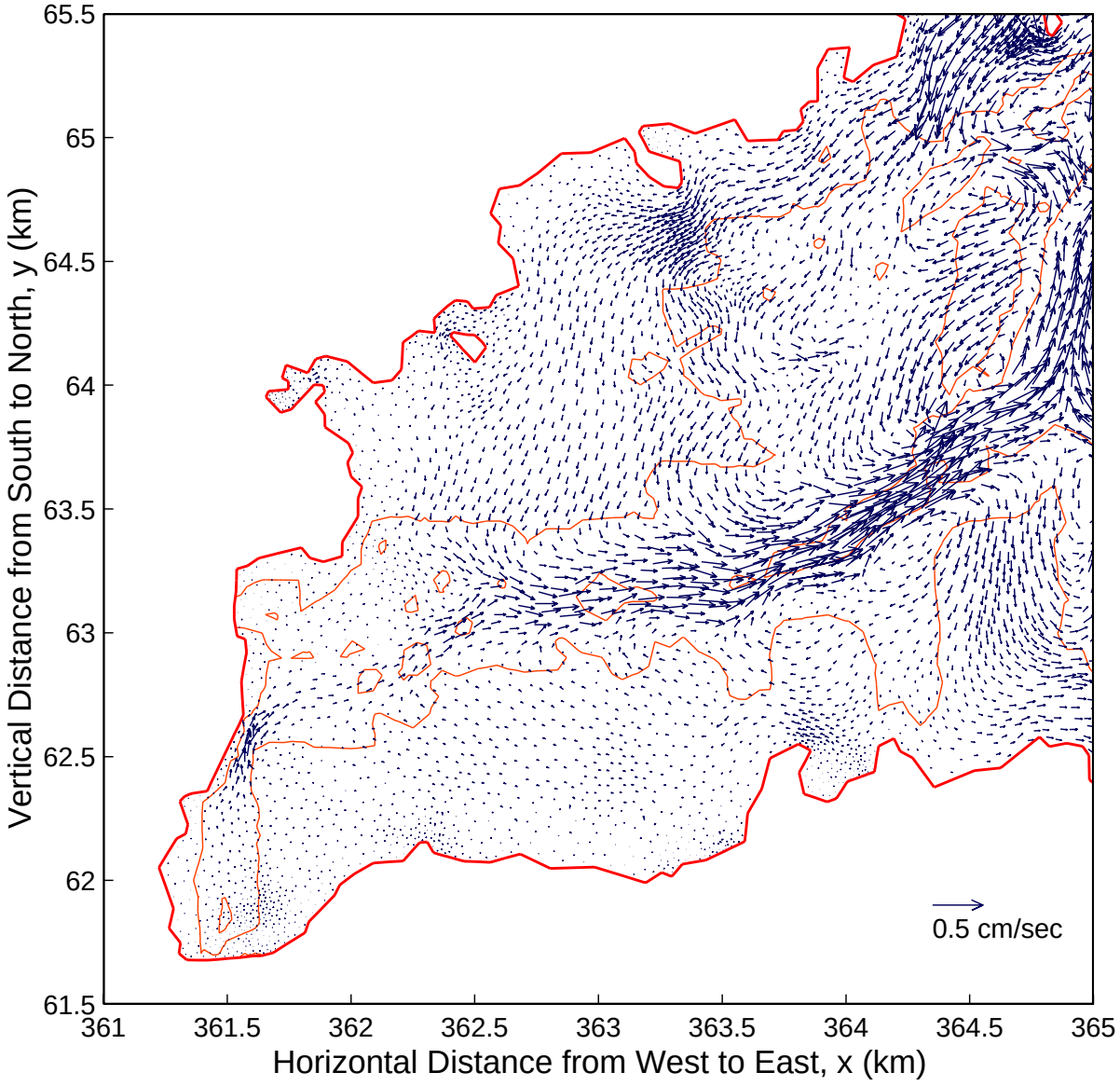

Figure 9: Residual M_2 velocity in southwestern Great Bay.

of the Frankfort Island, this ebb-oriented transport intersects with a flood-oriented transport in the center channel, which dominates the channel and flats of the middle Piscataqua. This suggests a depositional zone, which may be justified by the existence of the mud and coarse-grained Frankfort Island and an approximately 4 m deep shoal area in the vicinity of the convergence zone. In the mid-section of the Piscataqua River, there is a strong upriver transport from the constricted deeper channel at Boiling Rock (Figure **??**). This transport decreases considerably in the upriver direction and forms two small-amplitude gyres. This decrease is consistent with a shoal, consisting of upriver directed sand waves of about 2.9 m in height and 49m in wavelength, observed in this area (Bilgili *et al.*, 1996), since the sediment transport into the shoal area from downriver is much greater than that out upriver of the shoal. A sediment transport divergence zone predicted by the model at Boiling Rock may be acting as a nearby sediment source for the depositional area in the Piscataqua River. This divergence prediction is also consistent with an approximately 19 m deep trough observed just downriver from Boiling Rock.

In the lower section of the Piscataqua River and in Portsmouth Harbor, the general trend is a weak flood-oriented residual sediment transport on the shallow areas and flats and very strong ebb-oriented transport in the deep channels (Figure **??**). The magnitudes are especially high in the vicinity of Portsmouth Harbor. As the mouth of the estuary is reached, the residual bedload transport weakens but still continues to transport sediments out of the estuary. On the flats on the southwestern side of New Castle Island, the transport is weak and mostly flood-oriented with a relatively strong transport in the narrow Little Harbor channels due to high currents.

5 Discussion

The model is able to capture the highly dissipative regime in the Lower Piscataqua River and, to a lesser extent, the less dissipative standing character of the tidal wave in Little and Great Bay. There are, however, some discrepancies between simulation results and observed values, especially in the case of the tidal elevation amplitudes, which the model fails to simulate correctly beyond the Dover Point constriction. At this time, the slight increase in the M_2 amplitude beyond Dover Point that could not be replicated by the kinematic model is thought to be due to local accelerations. This idea is consistent with the usual standing wave solution for estuarine tides, which includes local acceleration as a non-negligible term.

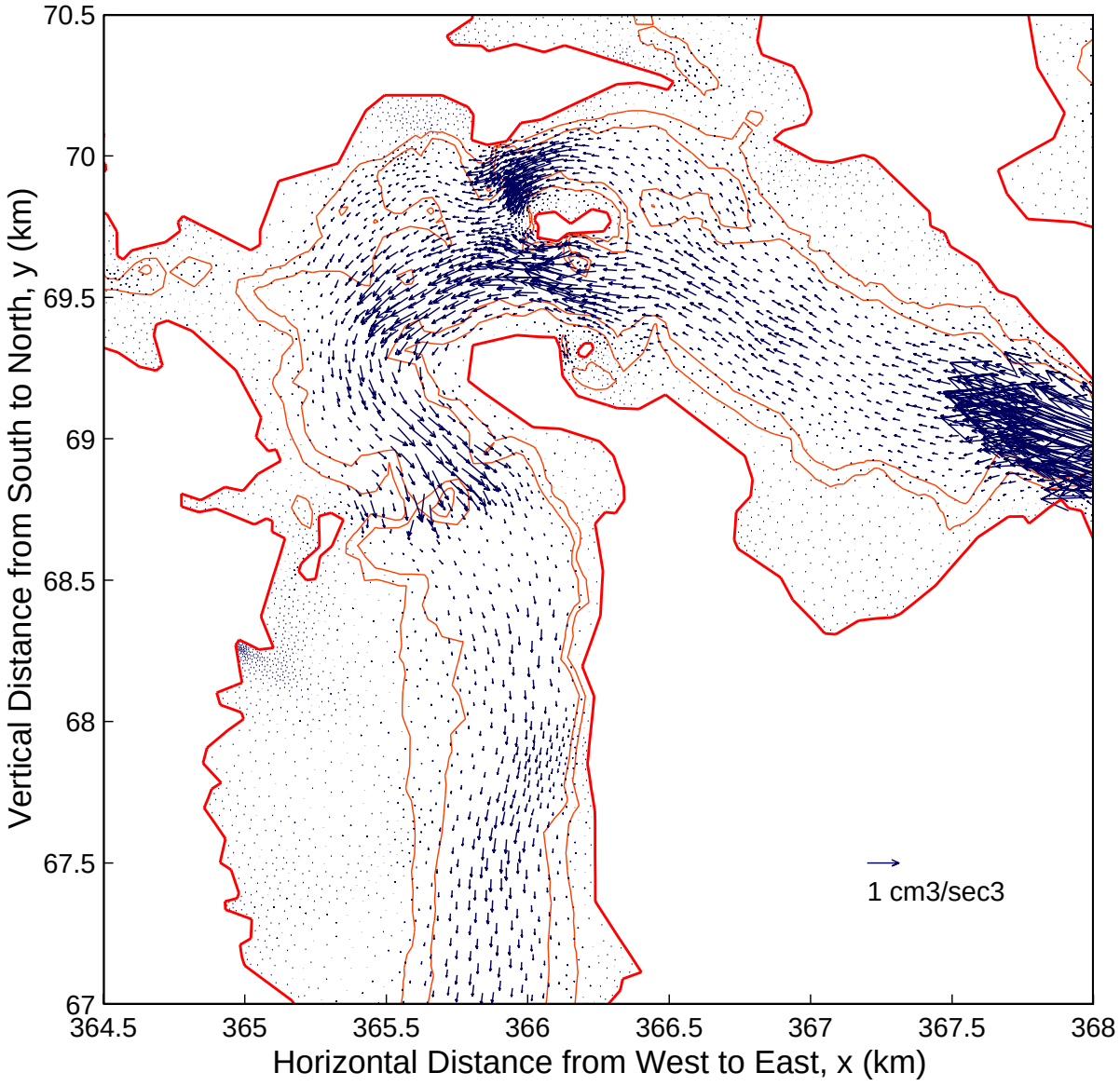

Figure 10: Model residual sediment transport in Little Bay.

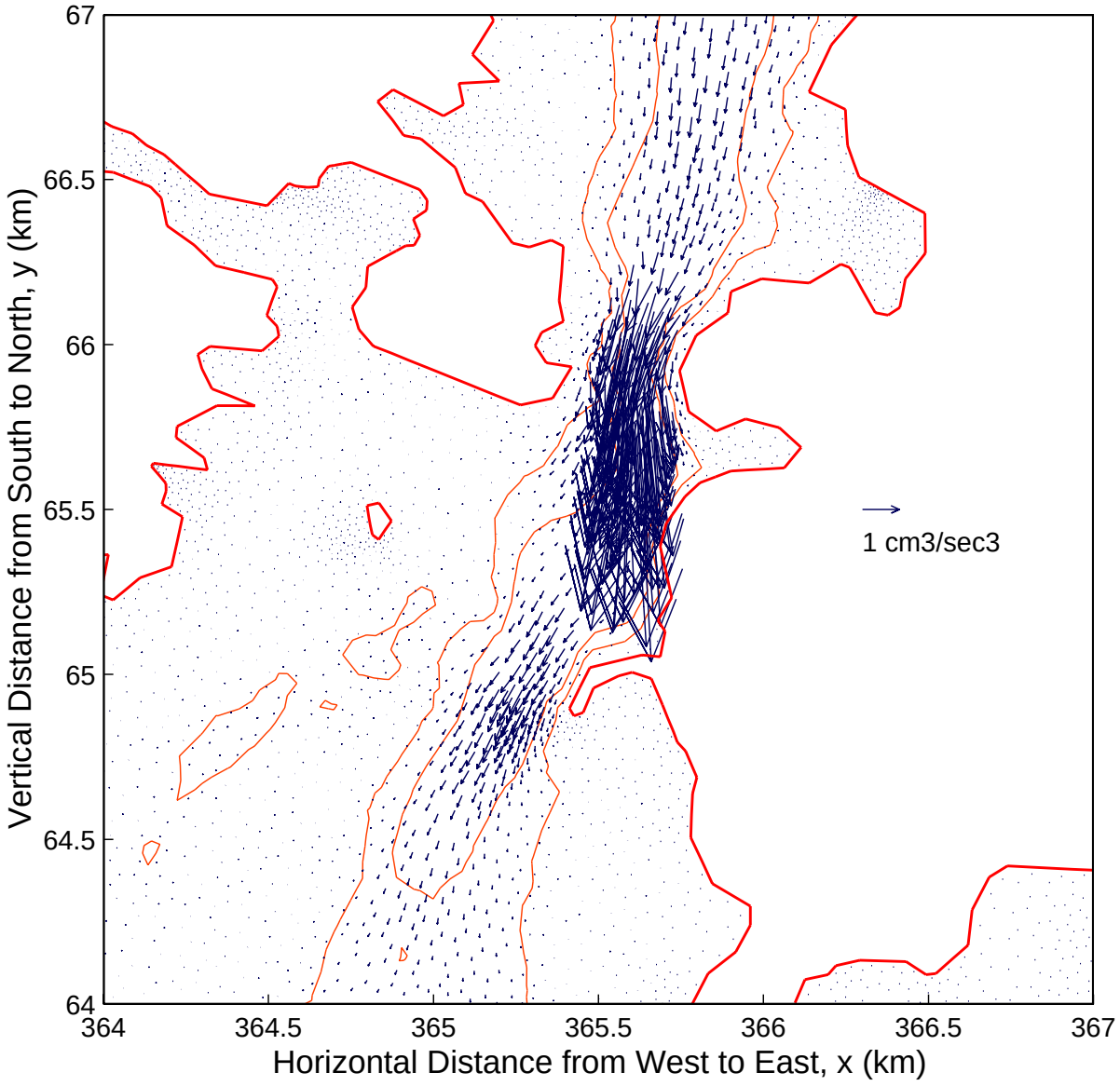

Figure 11: Model residual sediment transport in northern Great Bay.

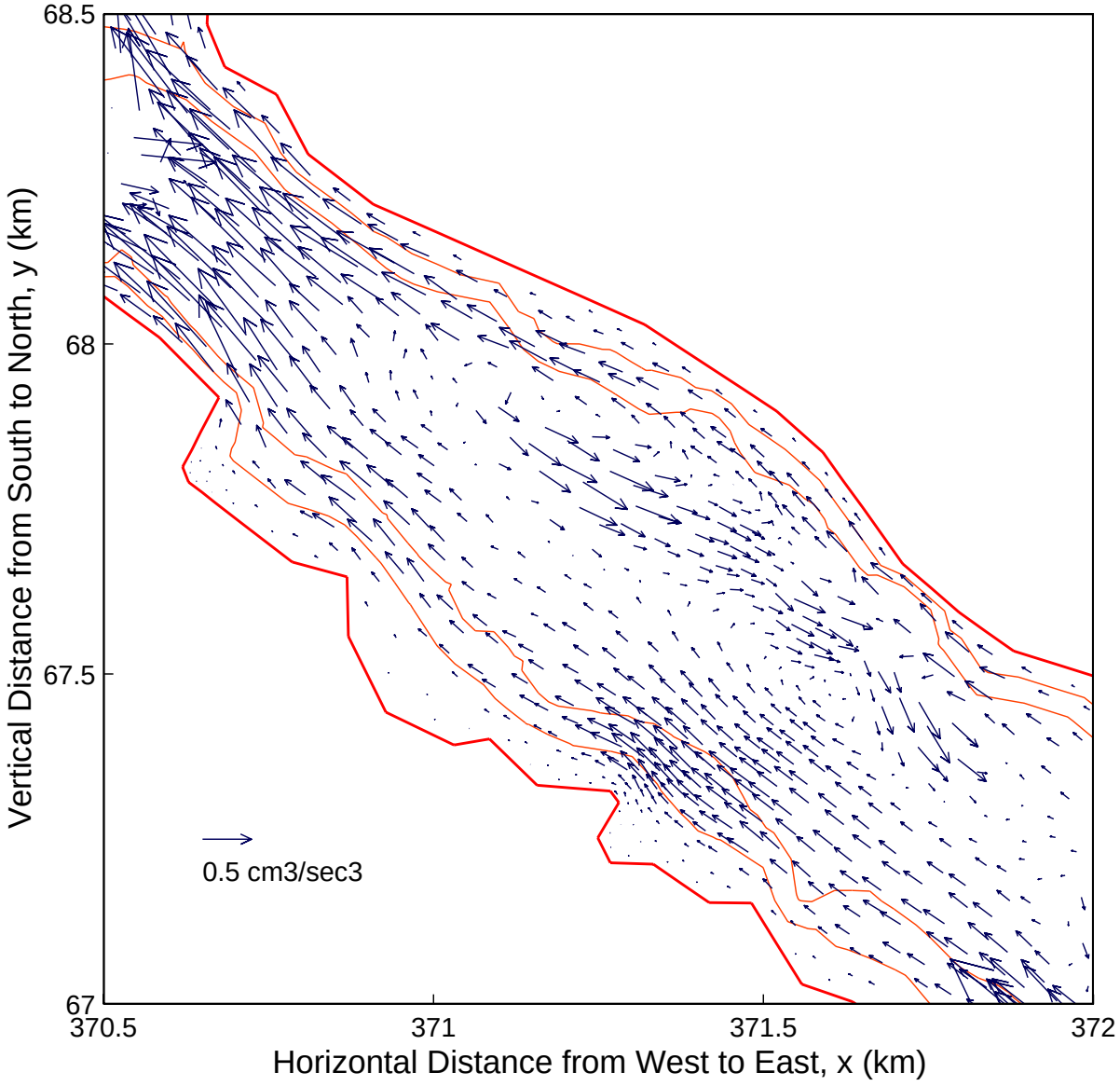

Figure 12: Model residual sediment transport in mid-section of Piscataqua.

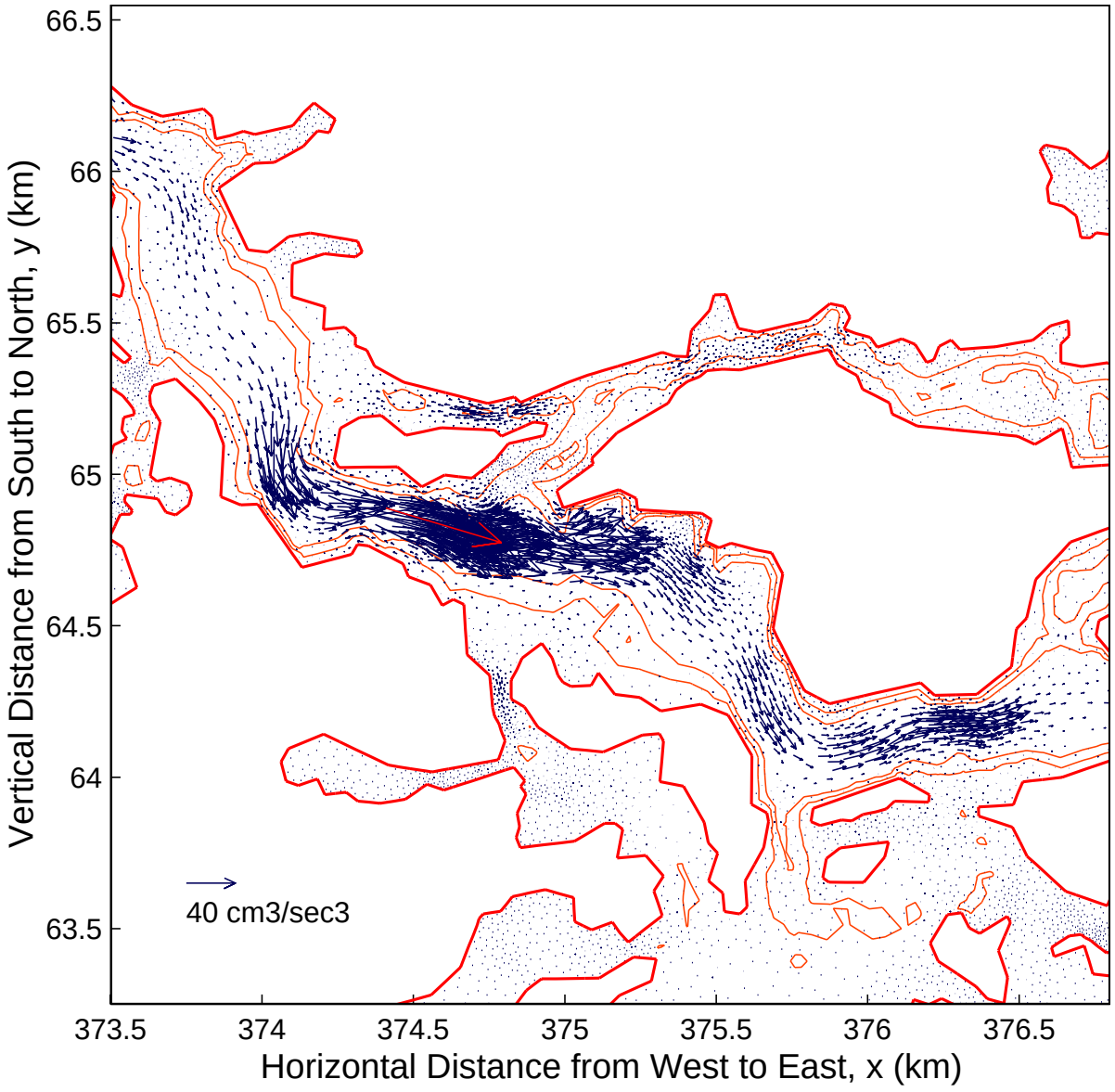

Figure 13: Model residual sediment transport in the Lower Piscataqua and Portsmouth Harbor.

Model results for cross-section averaged tidal current are in good agreement with corresponding time series generated using observed tidal constituents. The model is able to simulate the asymmetry between the flood and ebb stages successfully. The predicted pattern for residual current in channels with adjacent shallow areas (ebb-directed in the channel, flood-directed over the flats) has been recorded in similar estuaries. The distribution in the Great Bay System of a term proportional to bedload transport is consistent with several important bottom sediment and geological features.

These comparisons support the conclusion that the essential physics included in the model (i.e. the balance between the bottom friction and the pressure gradient) is sufficient for reliable predictions in the Lower Piscataqua River region where the kinematic assumption holds true. The method for incorporating watering-dewatering of the tidal flats realistically addresses continuity issues in a numerically stable manner. The success of this application depended strongly on accurate computation of the local drag coefficient, but was less sensitive to mesh element size.

Based on these results for a monochromatic M_2 forcing, future applications should add other tidal constituents to the basic M_2 contribution. Addition of the S_2 component is of particular interest since the spring-neap cycle could then be simulated. It is also planned to pursue the bedload transport implications. Lagrangian trajectories of sediment particles as well as specific bedload model applications having sediment-dependent parameters will be investigated.

6 Acknowledgements

We thank Mr. Zhitao Yu for his assistance in tidal analysis and prediction. Field observations were obtained as part of the Great Bay Estuarine Field Program under the New Hampshire Sea Grant College Program and NOAA. Financial support from the Cooperative Institute for Coastal and Estuarine Environmental Technology (grant numbers NA77OR0357, NA87OR0512, NA87OR338), NOAA/UNH is gratefully acknowledged.

References

Armstrong, P.B., G.M. Hanson, and H.E. Gaudette, Minor Elements in Sediments of Great Bay Estuary, New Hampshire, *Environmental Geology, 1*, 207–214, 1976.

Bilgili, A., M.R. Swift, and B. Celikkol, Shoal formation in the Piscataqua River, New Hampshire, *Estuaries*, *19*, 518–525, 1996.

Bowers, D.G., and A. Al-Barakati, Tidal rectification on drying estuarine sandbanks, *Estuaries*, *20*, 559–568, 1997.

Dennis, R.E., and E.E. Long, A user's guide to a computer program for the harmonic analysis at tidal frequencies, *NOAA Technical Report NOS41*, NOAA, Rockville, MD, 42pp., 1971.

Friedrichs, C.T., D.R. Lynch, and D.G. Aubrey, Velocity asymmetries in frictionally-dominated tidal embayments: longitudinal and lateral variability, *Dynamics and Exchanges in Estuaries and the Coastal Zone*, *Coastal and Estuarine Studies*, *Volume 40*, edited by D. Prandle, AGU, Washington D.C., 277–312, 1992.

Friedrichs, C.T., and O.S. Madsen, Nonlinear diffusion of the tidal signal in frictionally dominated embayments, *J. Geophys. Res.*, *97*, 5637–5650, 1992.

Garde, R.J., and K.G. Ranga Raju, *Mechanics of Sediment Transportation and Alluvial Stream Problems*, John Wiley and Sons Inc., New York, 618pp., 1985.

Ip, J.T.C., D.R. Lynch, and C.T. Friedrichs, Simulation of estuarine flooding and dewatering with application to Great Bay, New Hampshire, *Estuarine Coastal & Shelf Science*, *47*, 119–141, 1998.

Jago, C.F., and Y. Mahamod, A total load alghoritm for sand transport by fast steady currents, *Estuarine Coastal & Shelf Science*, *48*, 93–99, 1999.

Li, C., and J. O'Donnell, Tidally driven residual circulation in shallow estuaries with lateral depth variation, *Journal of Geological Research*, *102*, No. C13, 27915–27929, 1997.

Lin, B., and R.A. Falconer, Three-dimensional layer-integrated modelling of estuarine flows with flooding and drying, *Estuarine Coastal & Shelf Science*, *44*, 737–751, 1997.

Roberson, J.A., Cassidy, J.J., and Chaudry, M.H., *Hydraulic Engineering*, Houghton Mifflin Company, Boston, 114–118, 1988.

Short, F.T. (ed.), The ecology of the Great Bay Estuary, New Hampshire and Maine: An estuarine profile and bibliography, *NOAA-Coastal Ocean Program Publication*, 1992.

Simons, D.B., and F. Senturk, Sediment Transport Technology, *Water Resources Publications*, Fort Collins, Colorado, 807pp., 1977.

Swenson, E., W.S. Brown, and R. Trask, Great Bay Estuarine Field Program 1975 Data Report Part 1: Currents and Sea Levels, *UNH Sea Grant Technical Report*, UNH-SG-157, 109pp., 1977.

Swift, M.R., and W.S. Brown, Distribution of bottom stress and tidal energy dissipation in a well-mixed estuary, *Estuarine Coastal Shelf Sci.*, *17*, 297–317, 1983.

Van de Kreeke, J., and K. Robaczewska, Tide-induced residual transport of coarse sediment: Application to the Ems estuary, *Netherlands Journal of Sea Research*, *31-3*, 209–220, 1993.

Yalin, M.S., *Mechanics of Sediment Transport*, Pergamon Press Ltd., Oxford, England, 2nd Ed., 1977.